HHS Public Access

Author manuscript

Nature. Author manuscript; available in PMC 2013 December 13.

Published in final edited form as:

Nature. 2013 June 13; 498(7453): 224–227. doi:10.1038/nature12174.

RIP1-driven autoinflammation targets IL-1α independently of inflammasomes and RIP3

John R. Lukens[1], **Peter Vogel**[2], **Gordon R. Johnson**[1], **Michelle A. Kelliher**[3], **Yoichiro Iwakura**[4], **Mohamed Lamkanfi**[5,6,7], and **Thirumala-Devi Kanneganti**[1,7,*]

[1]Department of Immunology, St. Jude Children's Research Hospital, Memphis, TN, 38105, USA

[2]Animal Resources Center and the Veterinary Pathology Core, St. Jude Children's Research Hospital, Memphis, TN, 38105, USA

[3]Department of Cancer Biology, University of Massachusetts Medical School, Worcester, MA, 01605, USA

[4]Center for Experimental Medicine, Institute of Medical Science, University of Tokyo, Tokyo 108-8639, Japan

[5]Department of Medical Protein Research, VIB, B-9000 Ghent, Belgium

[6]Department of Biochemistry, Ghent University; B-9000 Ghent, Belgium

Abstract

The protein-tyrosine phosphatase SHP-1 plays critical roles in immune signaling, but how mutations in SHP-1 cause inflammatory disease in humans remains poorly defined[1]. Mice homozygous for the Y208N amino acid substitution in the carboxy-terminus of SHP-1 (referred to as *Ptpn6*^{spin} mice) spontaneously develop a severe inflammatory syndrome that resembles neutrophilic dermatosis in humans and is characterized by persistent footpad swelling and suppurative inflammation[2,3]. Here, we report that RIP1-regulated IL-1α production by hematopoietic cells critically mediates chronic inflammatory disease in *Ptpn6*^{spin} mice, whereas inflammasome signaling and IL-1β-mediated events were dispensable. IL-1α was also critical for exacerbated inflammatory responses and unremitting tissue damage upon footpad microabrasion of *Ptpn6*^{spin} mice. Intriguingly, pharmacological and genetic blockade of the kinase RIP1 protected against wound-induced inflammation and tissue damage in *Ptpn6*^{spin} mice, whereas RIP3 deletion failed to do so. Moreover, RIP1-mediated inflammatory cytokine production was attenuated by NF-κB and ERK inhibition. Together, our results suggest that wound-induced tissue

[*]**Correspondence should be addressed to:** Thirumala-Devi Kanneganti, Department of Immunology, St Jude Children's Research Hospital, MS #351, 570, St. Jude Place, Suite E7004, Memphis TN 38105-2794, Tel: (901) 595-3634; Fax. (901) 595-5766. Thirumala-Devi.Kanneganti@StJude.org.

[7]Contributed equally

Author Contributions

J.R.L., M.L., T.-D.K. designed the study; J.R.L. performed experiments and G.R.J. provided technical assistance, J.R.L., M.L. T.-D.K. analyzed data and wrote the manuscript. M.K., Y.I. provided genetic tools. P.V. performed and analyzed the histopathology data; T.-D.K oversaw the project.

Conflict of interest

The authors declare no competing financial interests.

damage and chronic inflammation in *Ptpn6*^{spin} mice are critically dependent on RIP1-mediated IL-1α production, whereas inflammasome signaling and RIP3-mediated necroptosis were dispensable. Thus, we have unravelled a novel inflammatory circuit in which RIP1-mediated IL-1α secretion in response to deregulated SHP-1 activity triggers an inflammatory destructive disease that proceeds independently of inflammasomes and programmed necrosis.

Keywords

SHP-1; *Ptpn6*; inflammasome; NOD-like receptor; caspase; interleukin; RIP1; RIP3; cell death; inflammation

---

Mutations in the non-receptor protein tyrosine phosphatase Src homology region 2 (SH2) domain-containing phosphatase-1 (SHP-1) are associated with a spectrum of inflammatory and autoimmune diseases in humans[4,5]. Similarly, *motheaten* null and hypomorphic alleles of *Ptpn6*, the gene encoding SHP-1, causes a myeloproliferative disease in mice that is characterized by chronic inflammation[6–9]. Despite being one of the first *in vivo* genetic models of inflammatory disease, the prevailing mechanism responsible for SHP-1-driven inflammation remains to be formally elucidated. Complete characterization of the molecular mechanism responsible for SHP-1-mediated disease has been hindered by the fact that *motheaten* mice are immunodeficient, develop devastating pneumonitis and glomerulonephritis, and die by 2–9 weeks of age[10]. Recently, a new SHP-1 mutant mouse line (referred to as *Ptpn6*^{spin} mice) that harbours an Y208N amino acid substitution in the carboxy-terminal SH2 domain of SHP-1 was described[3]. Mice homozygous for the hypomorphic *spin* allele develop a chronic inflammatory and autoimmune disease at 8–16 weeks of age that presents as persistent swelling and suppurative inflammation of the cutaneous footpad tissue (Fig. 1a)[3]. The popliteal lymph nodes (popLNs) that drain the inflamed feet display massive lymphomegaly and are composed of enhanced numbers of both lymphocytes and myeloid cells (Fig. 1b). In contrast, LNs that drain non-inflamed areas in *Ptpn6*^{spin} mice do not display lymphomegaly (Supplementary Fig. 1). Diseased *Ptpn6*^{spin} mice exhibit elevated levels of circulating cytokines and chemokines that are associated with granulopoiesis and neutrophil recruitment (Fig. 1c). Consistent with augmented production of granulopoietic factors, the inflammatory lesions in the footpads of mutant mice are dominated by neutrophils (Fig. 1d), and neutrophilia ensues in the periphery (Fig. 1e and Supplementary Fig. 2). Moreover, spontaneous disease progression in *Ptpn6*^{spin} mice is characterized by enhanced frequencies of inflammatory T cells that produce high levels of IL-17 and IFN-γ (Fig. 1f and Supplementary Fig. 3) and the accumulation of T cells that exhibit an effector/memory phenotype (CD44^{hi} CD62L^{lo}) (Supplementary Fig. 4). Analysis of mice before the onset of overt disease (4–8 weeks of age) reveals that *Ptpn6*^{spin} mice possess normal numbers of lymphoid and myeloid cells (Supplementary Fig. 5), and do not display perturbations in T cell development, regulatory T cell numbers, or T cell activation status before disease progression (Supplementary Fig. 6). Furthermore, the *Ptpn6*^{spin} mutation does not affect inflammatory cytokine production by peripheral T cells and other immune cells in young mutant mice (Supplementary Fig. 7).

Previous work established that interleukin (IL)-1 receptor (IL-1R) signalling is required for *Ptpn6*^{spin}-mediated inflammatory disease[3]. However, the molecular mechanisms operating upstream of IL-1R engagement that are responsible for spontaneous induction of inflammatory disease are not known. Inflammasome-driven activation of caspase-1 is increasingly recognized as a central instigator of inflammation and disease pathology through its critical role in the production of bioactive IL-1β[11]. In this context, the NLRP3 inflammasome responds to a multitude of damage-associated danger signals that are associated with autoinflammation[12]. To test whether aberrant inflammasome activation is responsible for inducing inflammatory disease in response to defective SHP-1 signaling, *Ptpn6*^{spin} mice were bred to animals that are deficient in the key inflammasome proteins NLRP3 and caspase-1. However, homozygous disruption of neither NLRP3 nor caspase-1 rescued *Ptpn6*^{spin} mice from footpad inflammation (Fig. 2a and Supplementary Fig. 8) and neutrophil infiltration (Fig. 2b). In full agreement, homozygous deletion of the gene encoding IL-1β also failed to prevent footpad inflammation and granulocyte recruitment in *Ptpn6*^{spin} mice (Fig. 2a, b and Supplementary Fig. 8). Nor was exorbitant inflammatory cytokine production and cutaneous inflammatory disease rescued by genetic deletion of TLR4 (Supplementary Fig. 9). In marked contrast, genetic ablation of IL-1α provided significant protection from the development of footpad inflammatory disease in *Ptpn6* mutant mice (Fig. 2a, b and Supplementary Fig. 8), which was associated with a return to normal neutrophil numbers (Fig. 2b–d), and reduced generation of T_H17 cells (Fig. 2e). These findings demonstrate that IL-1α plays a central role in SHP-1-mediated disease progression, which proceeds independently of inflammasome activation and IL-1β secretion.

Given that IL-1α acts an alarmin that orchestrates wound healing responses[13–15], we next tested whether defective wound healing might contribute to disease pathogenesis in *Ptpn6*^{spin} mice. To this end, mice were subjected to microabrasion injury on the plantar surfaces of the hind feet, and monitored for incidence of inflammatory responses. Microabrasion-provoked tissue damage induced similar erythema and edema in wildtype and *Ptpn6*^{spin} mice during the first 48 hours. However, inflammation at the wound site was fully resolved in wildtype mice by day 14, whereas *Ptpn6*^{spin} mice developed exacerbated inflammation that was characterized by intense redness and swelling of the affected area (Fig. 3a, b and Supplementary Fig. 10). At day 21, the inability of *Ptpn6*^{spin} mice to curtail wound inflammation ultimately resulted in the development of a persistent and aggravated state of footpad inflammation characterized by severe pustular dermatosis and edema (Fig. 3a, b and Supplementary Fig. 10). Notably, genetic ablation of IL-1α production in *Ptpn6*^{spin} mice provided full protection from microabrasion-induced footpad inflammation (Fig. 3a, b and Supplementary Fig. 10). The microabrasion procedure triggered a rapid (4–5 hrs post-wound induction) and potent production of inflammatory cytokines and chemokines in wildtype mice that was further exacerbated in *Ptpn6*^{spin} mice (Fig. 3c). Notably, the enhanced secretion of neutrophilic factors in *Ptpn6*^{spin} mice was fully rescued in *Ptpn6*^{spin} mice lacking IL-1α (Fig. 3c). Augmented wound healing responses in *Ptpn6*^{spin} mice were not the result of global aberrations in inflammation because young *Ptpn6*^{spin} mice did not display abnormalities in immune cell composition or inflammatory cytokine production (Supplementary Fig. 5–7). Furthermore, the *Ptpn6*^{spin} mutation did not affect the generation of MOG-specific T cells or neuroinflammation during experimental autoimmune

encephalomyelitis (EAE) in young mice (Fig. 3d, e and Supplementary Fig. 11). Commensal bacteria are increasingly recognized for their role in the pathogenesis of autoimmune diseases[16], and defects in innate immune signaling was recently shown to alter the intestinal microbiome[17]. Because inflammatory disease was suppressed when *Ptpn6*^{spin} mice were derived under germ-free conditions[3], we explored the possibility of footpad-associated dysbiosis in *Ptpn6*^{spin} mice. However, total bacterial counts and composition of the footpad-associated microbiome in microabrasion-induced inflammatory skin lesions were comparable in separately-housed wildtype and *Ptpn6*^{spin} mice, respectively (Supplementary Fig. 12). Furthermore, we failed to observe enhanced microabrasion-induced granulopoietic cytokine production in wildtype mice that have been co-housed with *Ptpn6*^{spin} mice (Supplementary Fig. 13), suggesting that the *Ptpn6*^{spin} mutation alters immune responses to normal commensals rather than modifying the bacterial ecology of inflammatory skin lesions. Notably, *Ptpn6*^{spin} mice also were hypersensitive in the acetaminophen (APAP)-induced liver injury model that is considered a model for sterile autoinflammation and wound healing responses[18]. IL-1α deletion provided significant protection from APAP-induced liver injury as evidenced by markedly reduced serum alanine aminotransferase (ALT) levels in APAP-challenged *Ptpn6*^{spin}x*Il1α*$^{-/-}$ mice (Fig. 3f). Together, these results suggest a critical role for IL-1α in both sterile and commensal-associated inflammatory and wound healing responses of *Ptpn6*^{spin} mice.

To determine whether SHP-1 regulates inflammatory responses in haematopoietic or radioresistant cells, bone marrow chimera mice were generated. Expression of the hypomorphic *Ptpn6*^{spin} allele in the haematopoietic compartment alone promoted spontaneous footpad inflammation (Fig. 4a) concomitant with augmented cytokine production (Fig. 4b) and neutrophilia (Supplementary Fig. 14). In contrast, chimera mice bearing the *Ptpn6*^{spin} mutation only in radioresistant cells failed to develop footpad inflammation (**data not shown**), suggesting that SHP-1 expression in bone marrow-derived immune cells rather than in non-haematopoietic cells (such as keratinocytes) is critical for induction of the autoinflammatory syndrome. Collectively, these findings suggest that unwarranted IL-1α release in response to dysregulated SHP-1 activity in haematopoietic cells plays a pivotal role in the induction of inflammatory disease. To identify the bone marrow-derived cell populations that are responsible for *Ptpn6*^{spin}-induced inflammation, we investigated inflammatory responses in isolated macrophages and neutrophils as these cell types have been shown to centrally regulate inflammatory and wound healing responses[19]. The *Ptpn6*^{spin} mutation did not influence inflammatory cytokine production in macrophages (Supplementary Fig. 15). Although *Ptpn6*^{spin} neutrophils produced slightly higher levels of the proinflammatory cytokines G-CSF and TNF-α in response to LPS stimulation, production of other pro-inflammatory mediators (KC, IL-6 and IL-1β) was normal in these cells (Supplementary Fig. 16). We therefore concluded that modest differences in neutrophils-associated cytokine production may contribute, but are unlikely to fully account for the striking inflammatory phenotype observed *in vivo*.

The kinase receptor-interacting protein 1 (RIP1) is emerging as a key regulator of inflammatory cytokine production and cellular stress[20,21]. To address the *in vivo* role of RIP1 in exacerbated inflammatory cytokine production, *Ptpn6*^{spin} mice were pretreated with

either vehicle control (PBS), the RIP1 kinase inhibitor necrostatin-1 (Nec-1) or the structurally-related inactive Nec1 analog (iNec)[22] before being subjected to microabrasion injury. Unlike iNec, Nec-1-mediated *in vivo* inhibition of RIP1 kinase activity markedly attenuated secretion of inflammatory mediators in *Ptpn6*^{spin} mice to levels comparable to those of wildtype mice (Fig. 4c), suggesting a critical role for RIP1 signaling in *Ptpn6*^{spin}-induced inflammatory disease. RIP1-deficient mice suffer from perinatal lethality[21], hampering genetic analysis of the role of RIP1 in *Ptpn6*^{spin}-induced autoinflammation. However, the observation that *Ptpn6*^{spin}-mediated autoinflammation stems from the haematopoietic compartment (Fig. 4a, b) provided a rationale to explore the role of RIP1 by means of fetal liver transplantation experiments. To this end, fetal liver cells from *Ptpn6*^{WT}*Rip1*$^{+/+}$, *Ptpn6*^{spin}*Rip1*$^{+/+}$ *and PTPN6*^{spin}*Rip1*$^{-/-}$ embryos collected at E14.5 were transferred into irradiated CD45.1 congenic mice. Reconstitution of recipient mice with control *Ptpn6*^{spin}*Rip1*$^{+/+}$ fetal liver cells resulted in unremitting footpad swelling, whereas genetic deletion of RIP1 in the haematopoietic compartment provided protection against *Ptpn6*^{spin}-associated inflammatory disease progression (Fig. 4d and Supplementary Fig. 17) and neutrophilia (Fig. 4e), a hallmark of this inflammatory syndrome. We hypothesized that targeted MAP kinase and NF-κB signaling to drive *Ptpn6*^{spin}-associated inflammation. In agreement, we found that *in vivo* RIP1 inhibition markedly dampened local activation of ERK and NF-κB signalling (Fig. 4f). Moreover, pharmacological blockade of NF-κB activation with the IKK-β inhibitor SC-514 and inhibition of ERK signalling with U0126 treatment both abrogated hyperinflammatory cytokine production in *Ptpn6*^{spin} mice (Supplementary Fig. 18). Importantly, the RIP1 kinase inhibitor Nec-1 also inhibited the synthesis of *Il1α* transcripts (Fig. 4g), further highlighting the role of RIP1 as a critical regulator of NF-κB-induced and IL-1α-driven autoinflammation in *Ptpn6*^{spin} mice. Notably, IL-1α deletion also attenuated exacerbated ERK and NF-κB signalling in the footpads of *Ptpn6*^{spin} mice (Fig. 4f), suggesting that RIP1-mediated IL-1α production triggers an inflammatory feedback loop that contributes to disease progression. In addition to driving MAP kinase and NF-κB activation, RIP1 controls necroptosis induction in conjunction with RIP3[20]. To verify a potential role for unwarranted necroptosis induction in *Ptpn6*^{spin}-associated inflammatory disease, *Rip3*-deficient mice were bred to *Ptpn6*^{spin} mice. However, unlike RIP1 and IL-1α deletion, genetic ablation of RIP3 expression failed to protect *Ptpn6*^{spin} mice from exacerbated inflammation in response to microabrasion-induced tissue injury (Fig. 4h and Supplementary Fig. 19). These results indicate that RIP3-mediated necroptosis is dispensable, and suggest a critical role for RIP1-mediated regulation of MAP kinase and NF-κB signalling in driving the inflammatory phenotype of *Ptpn6*^{spin} mice.

Defective neutrophil homeostasis is associated with numerous devastating human diseases[23]. For instance, neutropenia can cause severe susceptibility to infection, whereas neutrophilia is linked to autoinflammatory disorders. Our results in the *Ptpn6*^{spin} mouse inflammation model highlight a critical role for RIP1-mediated ERK and NF-κB signalling in hematopoietic cells in driving an inflammatory circuit that triggers exorbitant inflammatory responses and persistent tissue damage. Indeed, biochemical and genetic blockade of RIP1 signaling prevented inflammatory cytokine production and protected *Ptpn6*^{spin} mice from autoinflammation. IL-1α was critical for RIP1-mediated inflammatory disease progression, which proceeded independently of inflammasome/caspase-1-produced

IL-1β and RIP3-mediated necroptosis. Consequently, therapeutic inhibition of RIP1 activity and/or neutralization of IL-1α may provide novel approaches to break the self-reinforcing inflammatory circuits that drive chronic autoinflammatory and autoimmune diseases.

Methods Summary

Ptpn6^{spin} mice homozygous for the Y208N amino acid substitution in the c-terminal Src homology 2 domain of SHP-1 were previously described[3]. *Ptpn6*^{spin} mice spontaneously develop a persistent footpad disease that is characterized by paw swelling and cutaneous inflammation at 8–16 weeks of age. Blood was collected by submandibular venipuncture to measure the levels of circulating neutrophils and inflammatory cytokines. To assess T cell-mediated cytokine production, splenocytes and popLN cells were restimulated with PMA/ionomycin followed by intracellular flow cytometry staining. Formalin-preserved footpad samples were embedded in paraffin. Footpad infiltration by inflammatory cells and neutrophils was assessed in a blinded manner by a pathologist using H&E staining and neutrophil immunohistochemistry. The accumulation of immune cells in lymphoid organs was evaluated with the use of flow cytometry staining. To provoke microabrasion injury, mice were anesthetized and the plantar surfaces of their hind paws were irritated by gently rubbing with sterile sandpaper. Clinical scores were assigned based on edema, erythema, and weepy wound formation. The development of persistent footpad swelling was utilized to evaluate disease incidence over time. EAE was induced using MOG peptide, CFA, heat-inactivated *Mycobacterium tuberculosis* and *Bordetella pertussis* toxin. Neutrophils were purified from the bone marrow and stimulated with LPS. Fetal liver cells collected at embryonic day 14.5 were transplanted into lethally-irradiated wildtype mice to generate *Ptpn6*^{spin}x*Rip1*$^{-/-}$≫WT chimera mice.

Methods

Mice

Ptpn6^{spin} ([3]), *Nlrp3*$^{-/-}$ ([24]), *Casp1*$^{-/-}$([24]), *Il1β*$^{-/-}$ ([25]), *Il1α*$^{-/-}$ ([26]), *Rip3*$^{-/-}$ ([27]) and *Rip1*$^{-/-}$ ([21]) mice were previously described. All mice were housed under specific pathogen-free conditions within the Animal Resource Center at St. Jude Children's Research Hospital. Animal studies were conducted under protocols approved by the Institutional Animal Care and Use Committee of St. Jude Children's Research Hospital.

Histopathology

Formalin-preserved feet were processed and embedded in paraffin according to standard procedures. Sections (5 μm) were stained with hematoxylin and eosin (H&E) and examined by a pathologist blinded to the experimental groups. For immunohistochemistry, formalin-fixed paraffin-embedded tissues were cut into 4 μm sections and slides were stained with anti-Gr-1 to stain neutrophils in the footpads.

Microabrasion injury model

A novel microabrasion wound model was developed to evaluate the inflammatory response in a synchronized and controlled fashion. In this model, WT and disease-free *Ptpn6*^{spin} mice

(4-8 weeks old) were anesthetized and the plantar surfaces of the hind paws were irritated by gently rubbing with sterile sandpaper to induce physical trauma and microinjuries. Clinical scores were assigned daily based on the following scale: 0, no disease; 1, erythema; 2, erythema and mild swelling; 3, erythema, swelling, and crusty wound formation; 4 weepy wound formation and severe swelling. The development of persistent footpad swelling was utilized to evaluate disease incidence over time. The levels of proinflammatory mediators that are produced in response to microabrasion injury were measured in the serum 4-5 hrs after wound induction. For the *in vivo* necrostatin-1 experiments, mice were given either 50 μg necrostatin-1 (Nec-1) (Sigma-Aldrich) or 50 μg of an inactive control analog (iNec, Calbiochem) by the intraperitoneal route 1 hr before microabrasion irritation of the footpads. Circulating cytokine levels were measured in the serum 4-5 hrs later.

Experimental autoimmune encephalomyelitis (EAE)

Age- (5-8 weeks) and sex-matched mice were immunized subcutaneously with 100 μg $MOG_{35–55}$ peptide (MEVGWYRSPFSRVVHLYRNGK) emulsified in CFA (Difco Laboratories) with 500 μg *Mycobacterium tuberculosis* on day 0. Mice also received 200 ng pertussis toxin (List Biological Laboratories) by intraperitoneal injection on days 0 and 2. Disease severity was assessed daily by assigning clinical scores according to the following scale: 0, no disease; 1, tail paralysis; 2, weakness of hind limbs; 3, paralysis of hind limbs; 4, paralysis of hind limbs and severe hunched posture; 5, moribund or death. To harvest CNS leukocytes, mice were perfused through the left ventricle with PBS. The spinal cord was isolated, cut into small pieces, and then passed through a 70 μm cell strainer. Leukocytes were then purified by gradient centrifugation using a 38% Percoll solution. Cells were washed once in PBS and then resuspended in media.

In vivo serum cytokines

Blood was collected by submandibular venipuncture and allowed to clot for 30-60 minutes at room temperature. Serum was collected after centrifugation and cytokines were measured by ELISA.

ELISA

Cytokine ELISA was performed according to manufacturer's instructions (Millipore).

Flow cytometry and antibodies

The following monoclonal antibodies were used for flow cytometric cell marker analysis: CD4 (L3T4), IFN-γ (XMG1.2), IL-17A (eBio17B7), MHCII (M5/114.15.2), CD11b (M1/70), CD19 (6D5), CD44 (IM7), Ly-6G (1A8), CD25 (3C7), B220 (RA3-6B2), and Gr-1 (RB6-8C5) from eBioscience and TCR-β (H57-597), CD8 (53-6.7), Foxp3 (FJK-16s), CD62L (MEL-14), TNF-α (MP6-XT22), CD11c (N418), CD45.1 (A20), and CD45.2 (104) from Biolegend. Intracellular cytokine staining was done using the eBioscience IC fixation/ permeabilization kit according to the manufacturer's protocol. Intracellular staining for the Foxp3 transcription factor was performed using the eBioscience Foxp3 staining set according to the manufacturer's recommendations. Flow cytometry data were acquired on

an upgraded five-color FACScan or multi-color LSRII (BD) and were analyzed with FlowJo software (TreeStar).

Ex vivo lymphocyte restimulation

Splenocytes and LN (popliteal and mesenteric) cells were harvested and restimulated with 20 ng/ml phorbol 12-myristate 13-acetate (PMA) and 500 ng/ml ionomycin in the presence of monensin for 3-4 hrs. Cells were stained according to the manufacturer's instructions (eBioscience). For the EAE experiment, splenocytes were harvested and restimulated with 30 μg/ml MOG peptide. Supernatants were collected after 48 hrs to measure cytokine levels by ELISA.

Bone marrow chimeras

Bone marrow was flushed from the femurs and filtered through a 40 μm filter. 3-5 × 10^6 cells in 200 μl PBS were transferred by tail vein injection into lethally irradiated (1,000 rad) mice. Congenic CD45 markers were utilized to verify chimerism.

In vitro macrophage stimulation

Bone marrow derived macrophages (BMDMs) were generated by culturing bone marrow cells in L-cell-conditioned IMDM medium supplemented with 10% FBS, 1% nonessential amino acid, and 1% penicillin-streptomycin for 5 days. BMDMs were seeded in 12-well cell culture plates and cultured overnight. To evaluate cytokine production, BMDMs were primed with 2 μg/ml ultrapure *Escherichia coli*-derived LPS (Invivogen) for 3 hours followed by 5 mM ATP (Sigma-Aldrich) for an additional 30 min. BMDMs were also separately stimulated with *Salmonella typhimurium* (5 MOI) for 4 hr and supernatants were collected to evaluate cytokine secretion by ELISA.

Neutrophil culture and *in vitro* stimulation

Bone marrow cells were isolated from the femurs of mice and neutrophils ($CD11b^+$ $Gr\text{-}1^+$) were purified by flow cytometry sorting. Neutrophils (1×10^6 cells/ml) were stimulated with 100 ng/ml ultrapure *Escherichia coli*-derived LPS (Invivogen). Supernatants were collected after 48 hrs of stimulation and cytokine levels were measured by ELISA.

Western blotting

Footpad protein lysates were collected in RIPA lysis buffer supplemented with complete protease inhibitor cocktail (Roche) and PhosSTOP (Roche) using a tissue homogenizer. Samples were resolved by SDS-PAGE and transferred to polyvinylidene difluoride (PVDF) membranes via electroblotting. Membranes were blocked in 5% non-fat milk and incubated overnight at 4°C with primary antibodies. The membranes were then probed with horseradish peroxidase (HRP)-tagged secondary antibodies at room temperature for 1 hr. Immunoreactive proteins were visualized using the ECL method (Pierce).

Real-time RT-PCR

Total RNA was isolated from the hind paws with Trizol (Invitrogen) according to the manufacturer's instructions. 1 μg of RNA was reverse-transcribed to cDNA with random

RNA-specific primers using the high-capacity cDNA reverse transcription kit (Applied Biosystems). Transcript levels of *Il1α* and *Gapdh* were analyzed using SYBR-Green (Applied Biosystems) on an ABI7500 real-time PCR machine according to the manufacturers' recommendations. Relative expression was calculated using the delta-delta Ct standardization method.

Footpad pathology scoring

Footpad H&E sections were scored based on the extent and severity of inflammation, ulceration, and hyperplasia of the mucosa in a blinded fashion by a veterinary pathologist. Severity scores for inflammation were as follows: 0 = normal (within normal limits); 1 = minimal (small, focal, or widely separated); 2 = mild; 3 = moderate (moderate multifocal inflammation with dermatitis, suppurative, coalescing with intraepithelial and follicular abcesses); 4 = marked (marked inflammation, with intraepidermal pustules, epidermal hyperplasia, acantholysis, dermatitis, perifolliculitis); 5 = severe (severe inflammation, with intraepidermal pustules, epidermal hyperplasia, acantholysis, dermatitis, perifolliculitis, lesions covering >50% of the section).

APAP-induced hepatotoxicity model

Acetaminophen (Sigma-Aldrich) was dissolved in sterile PBS by heating the solution to 55°C. Mice that fasted overnight for 16-18 hrs received 250 mg/kg of acetaminophen (APAP) by intraperitoneal injection. Mice were harvested 18-20 hrs post injection and the levels of serum alanine aminotransferase (sALT) were measured in the blood by ELISA.

Statistical analysis

All results are presented as means ± standard errors. We performed statistical analysis using the two-tailed Student's *t*-test. Differences were considered statistically significant when $P<0.05$. *P* values are denoted by $*P<0.05$, $**P<0.01$, $***P<0.001$.

Supplementary Material

Refer to Web version on PubMed Central for supplementary material.

Acknowledgements

We thank B.A. Buetler, V.M. Dixit and D.R. Green for generous supply of mutant mice. We thank R. Weinlich for helpful discussions. We thank M. Johnson in the St. Jude Small Animal Imaging Center for helping to evaluate embryonic development in fetal liver transplantation studies. ML is supported by European Union Marie-Curie grant 256432, ERC Grant 281600, and grants G030212N, 1.2.201.10.N.00, and 1.5.122.11.N.00 from the Fund for Scientific Research-Flanders. This work was supported by grants from the National Institute of Health (Grants AR056296, CA163507 and AI101935) and the American Lebanese Syrian Associated Charities (ALSAC) to T.-D.K.

Abbreviations

IL	interleukin
Nec-1	necrostatin-1

NLR	NOD-like receptor
RIP	Receptor-Interacting Protein
SH2	Src Homology 2
WT	wildtype

References

1. Pao LI, Badour K, Siminovitch KA, Neel BG. Nonreceptor protein-tyrosine phosphatases in immune cell signaling. Annu Rev Immunol. 2007; 25:473–523. [PubMed: 17291189]
2. Nesterovitch AB, et al. Spontaneous insertion of a b2 element in the ptpn6 gene drives a systemic autoinflammatory disease in mice resembling neutrophilic dermatosis in humans. Am J Pathol. 2011; 178:1701–1714. [PubMed: 21435452]
3. Croker BA, et al. Inflammation and autoimmunity caused by a SHP1 mutation depend on IL-1, MyD88, and a microbial trigger. Proc Natl Acad Sci U S A. 2008; 105:15028–15033. [PubMed: 18806225]
4. Cao H, Hegele RA. Identification of polymorphisms in the human SHP1 gene. J Hum Genet. 2002; 47:445–447. [PubMed: 12181644]
5. Christophi GP, et al. SHP-1 deficiency and increased inflammatory gene expression in PBMCs of multiple sclerosis patients. Lab Invest. 2008; 88:243–255. [PubMed: 18209728]
6. Green MC, Shultz LD. Motheaten, an immunodeficient mutant of the mouse. I. Genetics and pathology. J Hered. 1975; 66:250–258. [PubMed: 1184950]
7. Shultz LD, Coman DR, Bailey CL, Beamer WG, Sidman CL. "Viable motheaten," a new allele at the motheaten locus. I. Pathology. Am J Pathol. 1984; 116:179–192. [PubMed: 6380298]
8. Shultz LD, et al. Mutations at the murine motheaten locus are within the hematopoietic cell protein-tyrosine phosphatase (Hcph) gene. Cell. 1993; 73:1445–1454. [PubMed: 8324828]
9. Tsui HW, Siminovitch KA, de Souza L, Tsui FW. Motheaten and viable motheaten mice have mutations in the haematopoietic cell phosphatase gene. Nat Genet. 1993; 4:124–129. [PubMed: 8348149]
10. Lorenz U. SHP-1 and SHP-2 in T cells: two phosphatases functioning at many levels. Immunol Rev. 2009; 228:342–359. [PubMed: 19290938]
11. Lukens JR, Dixit VD, Kanneganti TD. Inflammasome activation in obesityrelated inflammatory diseases and autoimmunity. Discov Med. 2011; 12:65–74. [PubMed: 21794210]
12. Tschopp J, Schroder K. NLRP3 inflammasome activation: The convergence of multiple signalling pathways on ROS production? Nat Rev Immunol. 2010; 10:210–215. [PubMed: 20168318]
13. Chen CJ, et al. Identification of a key pathway required for the sterile inflammatory response triggered by dying cells. Nat Med. 2007; 13:851–856. [PubMed: 17572686]
14. Cohen I, et al. Differential release of chromatin-bound IL-1alpha discriminates between necrotic and apoptotic cell death by the ability to induce sterile inflammation. Proc Natl Acad Sci U S A. 2010; 107:2574–2579. [PubMed: 20133797]
15. Rider P, et al. IL-1alpha and IL-1beta recruit different myeloid cells and promote different stages of sterile inflammation. J Immunol. 2011; 187:4835–4843. [PubMed: 21930960]
16. Kranich J, Maslowski KM, Mackay CR. Commensal flora and the regulation of inflammatory and autoimmune responses. Semin Immunol. 2011; 23:139–145. [PubMed: 21292499]
17. Henao-Mejia J, et al. Inflammasome-mediated dysbiosis regulates progression of NAFLD and obesity. Nature. 2012; 482:179–185. [PubMed: 22297845]
18. Kubes P, Mehal WZ. Sterile inflammation in the liver. Gastroenterology. 2012; 143:1158–1172. [PubMed: 22982943]
19. Chen GY, Nunez G. Sterile inflammation: sensing and reacting to damage. Nat Rev Immunol. 2010; 10:826–837. [PubMed: 21088683]

20. Vandenabeele P, Declercq W, Van Herreweghe F, Vanden Berghe T. The role of the kinases RIP1 and RIP3 in TNF-induced necrosis. Sci Signal. 2010; 3:re4. [PubMed: 20354226]
21. Kelliher MA, et al. The death domain kinase RIP mediates the TNF-induced NFkappaB signal. Immunity. 1998; 8:297–303. [PubMed: 9529147]
22. Takahashi N, et al. Necrostatin-1 analogues: critical issues on the specificity, activity and in vivo use in experimental disease models. Cell Death Dis. 2012; 3:e437. [PubMed: 23190609]
23. Amulic B, Cazalet C, Hayes GL, Metzler KD, Zychlinsky A. Neutrophil function: from mechanisms to disease. Annu Rev Immunol. 2012; 30:459–489. [PubMed: 22224774]

References to Methods section

24. Kanneganti TD, et al. Bacterial RNA and small antiviral compounds activate caspase-1 through cryopyrin/Nalp3. Nature. 2006; 440:233–236. [PubMed: 16407888]
25. Shornick LP, et al. Mice deficient in IL-1beta manifest impaired contact hypersensitivity to trinitrochlorobenzone. J Exp Med. 1996; 183:1427–1436. [PubMed: 8666901]
26. Matsuki T, Nakae S, Sudo K, Horai R, Iwakura Y. Abnormal T cell activation caused by the imbalance of the IL-1/IL-1R antagonist system is responsible for the development of experimental autoimmune encephalomyelitis. Int Immunol. 2006; 18:399–407. [PubMed: 16415102]
27. Newton K, Sun X, Dixit VM. Kinase RIP3 is dispensable for normal NF-kappa Bs, signaling by the B-cell and T-cell receptors, tumor necrosis factor receptor 1, and Toll-like receptors 2 and 4. Mol Cell Biol. 2004; 24:1464–1469. [PubMed: 14749364]

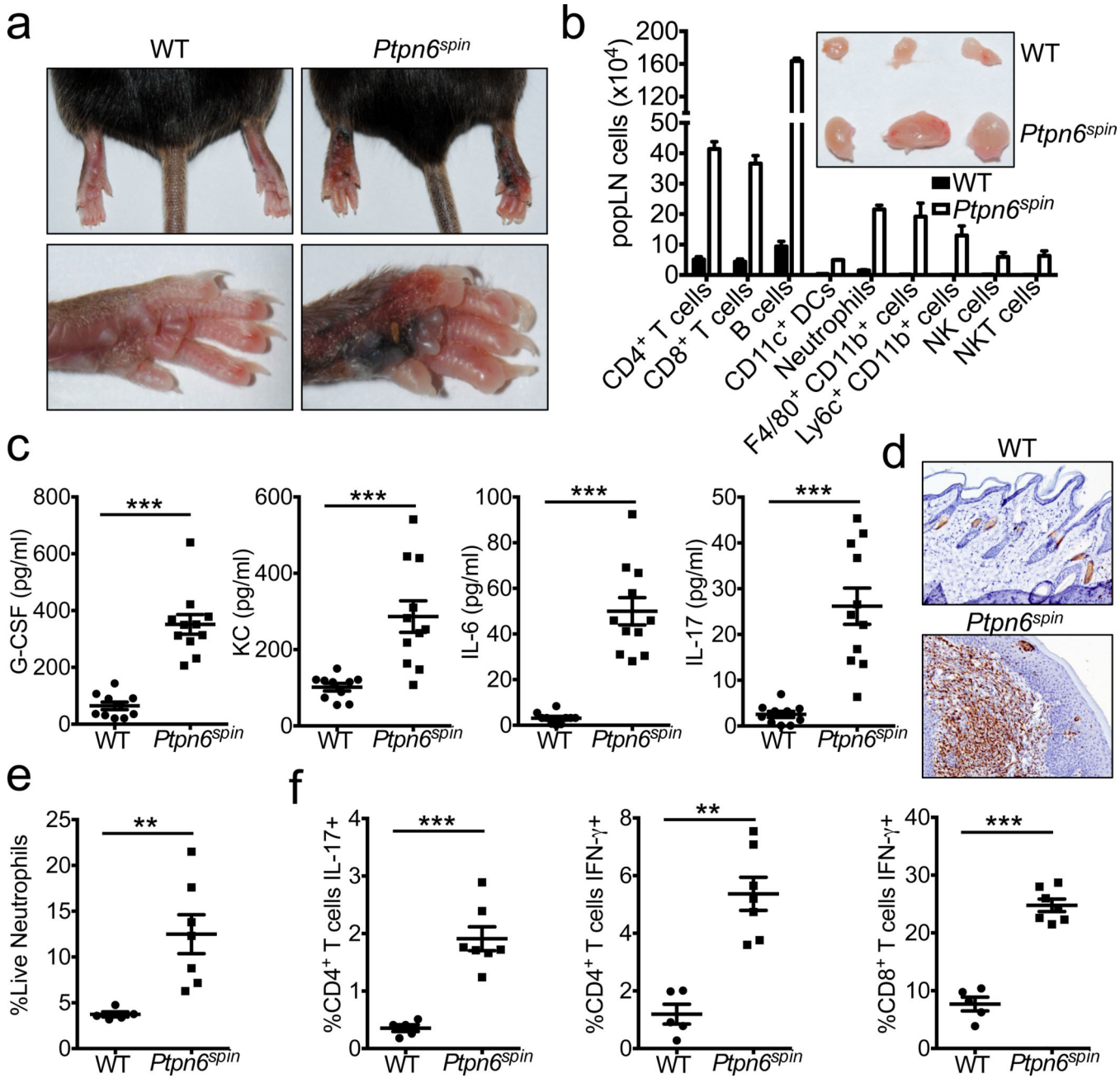

Figure 1. *Ptpn6*^{spin} mice develop spontaneous footpad inflammation

a–b, Spontaneous induction of footpad swelling (**a**) and lymphomegaly (**b**) in the popliteal lymph nodes (popLN) of *Ptpn6*^{spin} mice at 10–16 weeks of age. **b–f,** Wild-type (WT) and diseased *Ptpn6*^{spin} mice were harvested at 10–12 weeks of age. **b,** Numbers (mean ± s.e.m.) of popLN cells. Inset shows representative pictures of popLNs. **c,** Serum levels of cytokines and chemokines. **d,** Immunohistochemistry staining of neutrophils in the footpads. **e,** Frequency of splenocytes that are neutrophils. **f,** Production of IL-17 and IFN-γ by popLN CD4$^+$ and CD8$^+$ T cells following *in vitro* restimulation. Each point represents an individual

mouse, and the line represents the mean ± s.e.m. *$P < 0.05$, **$P < 0.01$, ***$P < 0.001$. DCs, dendritic cells. Tregs, regulatory T cells. NK, natural killer.

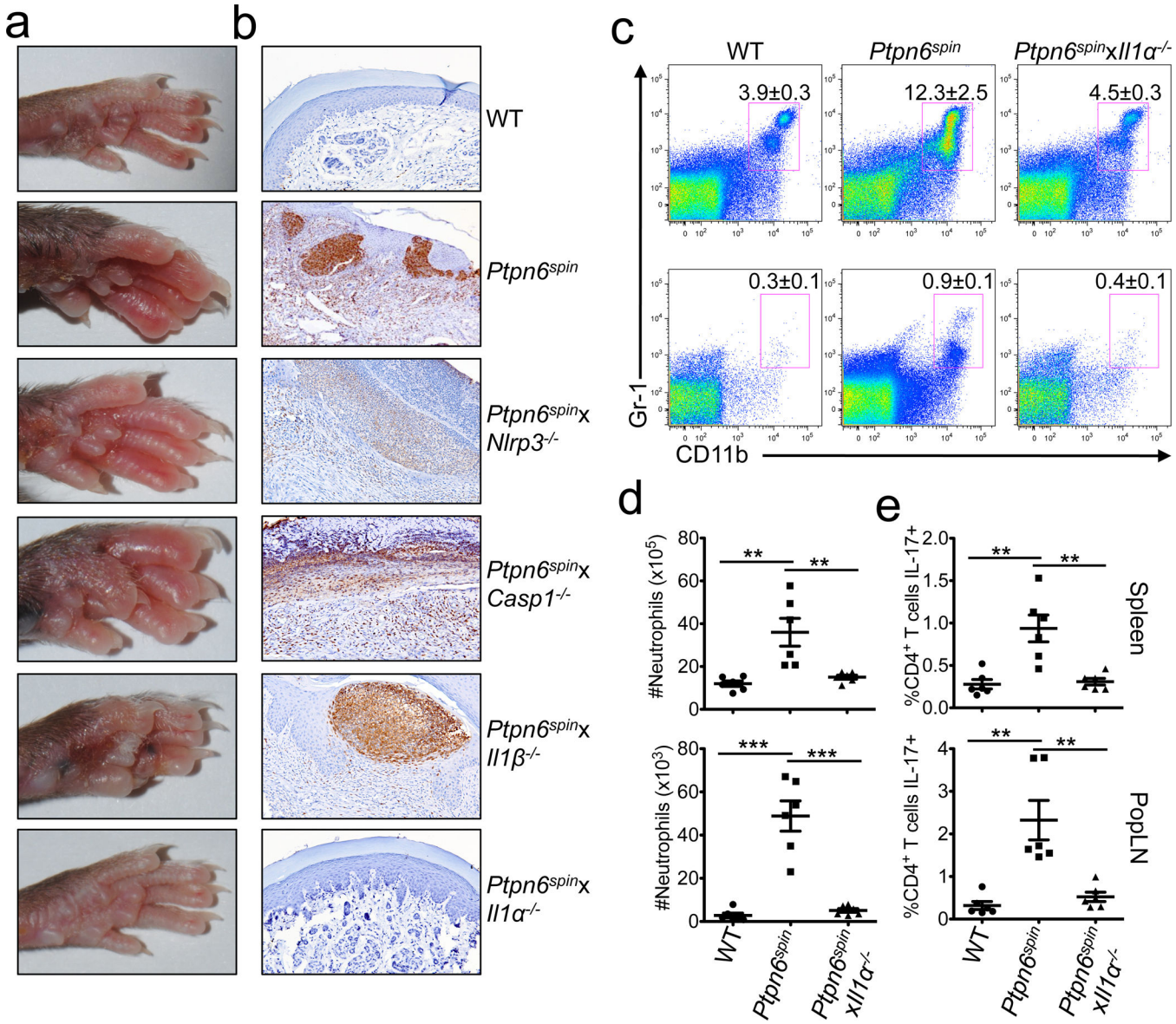

Figure 2. Deletion of IL-1α limits *Ptpn6*^{spin}-mediated disease

a–b, Footpad images (**a**), and neutrophil immunohistochemistry staining (**b**) of WT and *Ptpn6*^{spin} mice that were crossed with mice that are deficient in either NLRP3, Caspase-1, IL-1β, or IL-1α. **c–e,** Spleen and popLNs from 12–16 week old WT, *Ptpn6*^{spin}, and *Ptpn6*^{spin}x*Il1a*$^{-/-}$ mice. **c,** Frequencies of neutrophils in the spleen (top panel) and popLNs (bottom panel). Numbers in the FACs plots denote the mean frequencies ± s.e.m. of cells that are neutrophils. **d**, Total numbers of neutrophils in the spleen (top panel) and popLNs (bottom panel). **e,** Production of IL-17 by CD4^{+} T cells following *in vitro* restimulation. Data show mean ± s.e.m. Each point represents an individual mouse, and the line represents the mean ± s.e.m. *$P < 0.05$, **$P < 0.01$, ***$P < 0.001$.

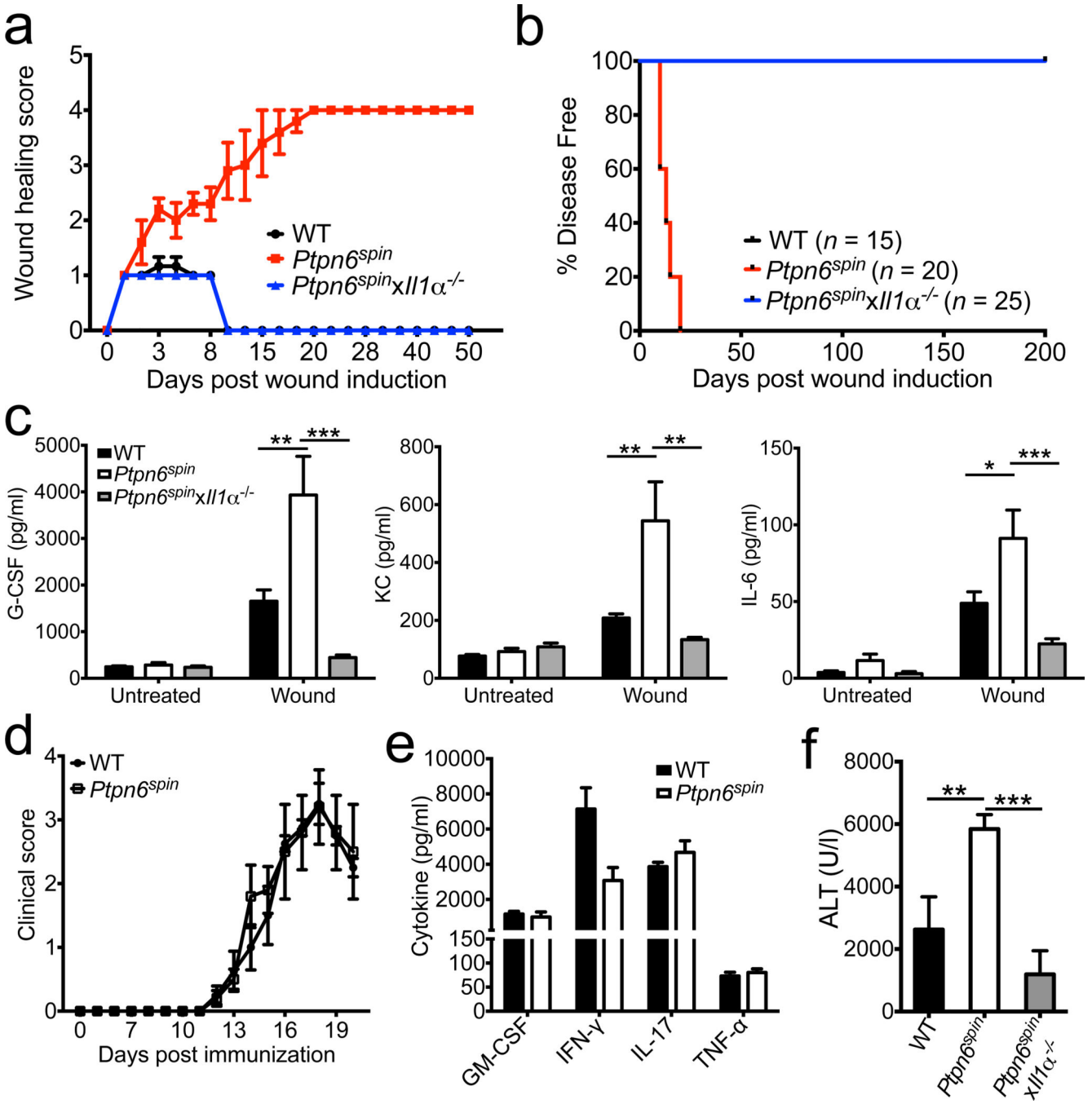

Figure 3. Exacerbated wound healing responses contribute to disease in *Ptpn6*^{spin} mice

a–c, Microabrasion injuries were induced on the plantar surfaces of the footpads of WT, *Ptpn6*^{spin}, and *Ptpn6*^{spin}x*Il1α*$^{-/-}$ mice. **a,** Clinical scores based on erythema and edema as described in detail in the methods section were recorded daily. **b,** Percentage of disease free mice over time. **c,** Serum levels of granulopoiesis-associated factors 5 hrs post microabrasion stimulation. **d–e**, WT (n = 4) and disease-free PTPN6 mutant mice (5–7 weeks old) (n = 5) were immunized with MOG/CFA and pertussis toxin. **d**, Mean clinical paralysis scores. **e**, Splenocytes were harvested on day 20 and restimulated with MOG

peptide for 48 hrs to measure cytokine secretion. **f**, WT (n = 7), disease-free (4–7 weeks of age) *Ptpn6*^{spin} (n = 9), and *Ptpn6*^{spin}x*Il1a*$^{-/-}$ (n = 5) mice received 250 mg/kg of acetaminophen by intraperitoneal injection. The levels of serum alanine aminotransferase (sALT) were measured 18–20 hours later by ELISA. All bar graphs show mean ± s.e.m. *P < 0.05, **P < 0.01, ***P < 0.001.

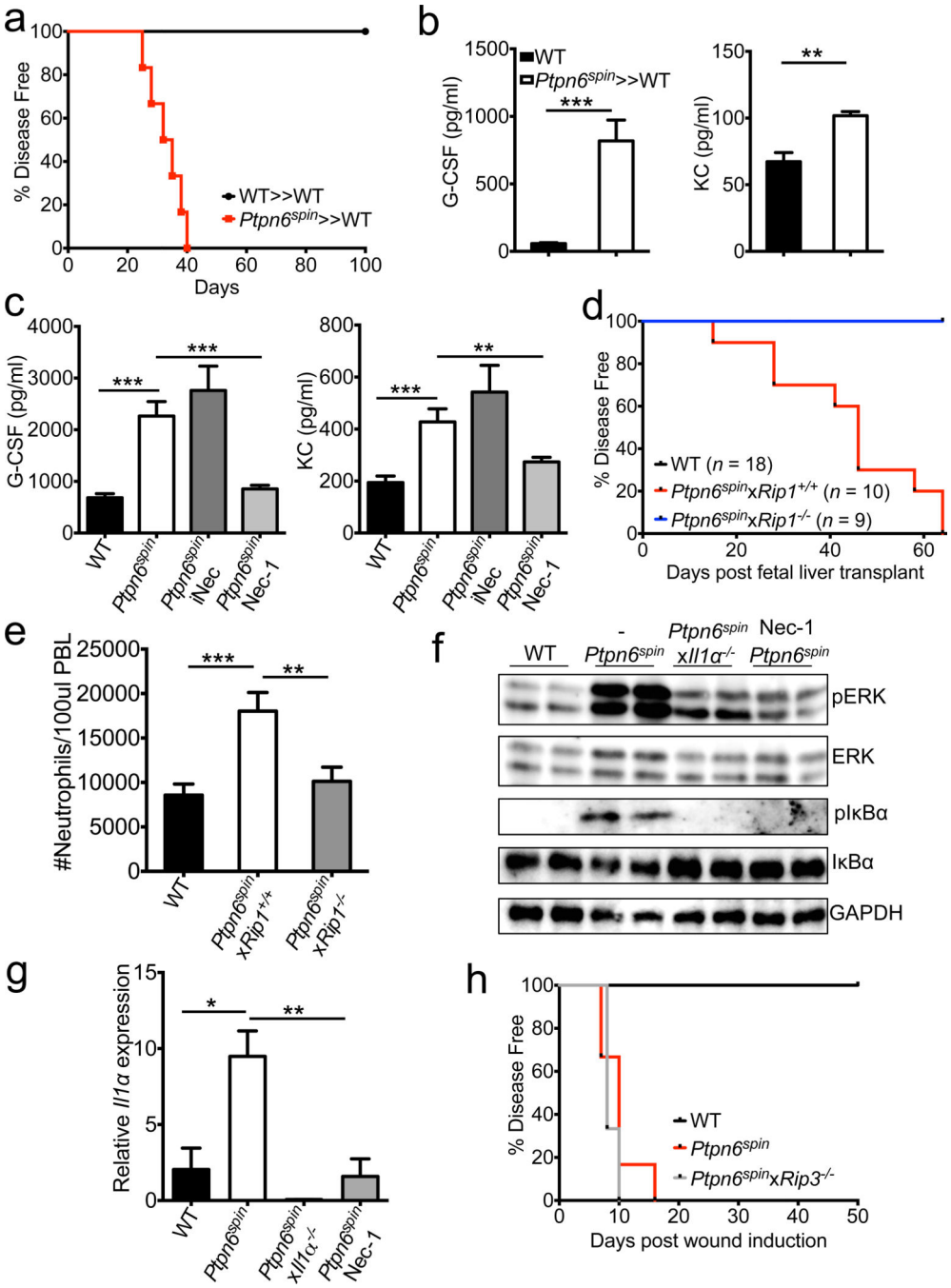

Figure 4. RIP1 regulates *Ptpn6*^{spin}-mediated disease through the control of proinflammatory signalling and *Il1α* expression and not via RIP3-induced necroptosis

a, Spontaneous incidence of footpad inflammation in bone marrow chimera mice (donor≫recipient). **b,** Levels of circulating granulopoiesis-associated factors in bone marrow chimeras. **c,** WT mice were preteated with vehicle control (n = 27) and *Ptpn6*^{spin} mice were pretreated with vehicle control (n = 22), 50 μg necrostatin 1 (Nec-1) (n = 33), or 50 μg of an inactive control analog of Nec-1 (iNec) (n = 10) for 1 hour before microabrasion injury induction. Serum levels of granulopoiesis-inducing factors 4 hrs post wound

induction. **d–e**, Spontaneous incidence of footpad inflammation (**d**) and numbers of peripheral blood neutrophils (**e**) in WT (*Ptpn6*^{WT}x*Rip1*$^{+/+}$ ≫ WT), *Ptpn6*^{spin}x*Rip1*$^{+/+}$ (*Ptpn6*^{spin}x*Rip1*$^{+/+}$ ≫ WT), and *Ptpn6*^{spin}x*Rip1*$^{-/-}$(*Ptpn6*^{spin}x*Rip1*$^{-/-}$ ≫ WT) fetal liver transplant mice. **f–g**, WT, *Ptpn6*^{spin}, and *Ptpn6*^{spin}x*Il1α*$^{-/-}$ mice were pretreated with PBS or 50 μg Nec-1 1 hour before microabrasion injury induction. Regulation of ERK and NF-κB signalling (**f**) and *Il1α* expression (**g**) in the footpads 2 hours post wound induction. **h**, Microabrasion injuries were induced on the plantar surfaces of the footpads of WT, *Ptpn6*^{spin}, and *Ptpn6*^{spin}x*Rip3*$^{-/-}$ mice. Percentages of disease free mice over time. Data show mean ± s.e.m. of a representative experiment. **P* < 0.05, ***P* < 0.01, ****P* < 0.001.